6-2016

# Supramolecular Assembly of Metal-Organic Tubes Constructed from the Ditopic Heteroscorpionate Ligand (4-$NH_2C_6H_4$)$CHpz_2$ (pz = Pyrazol-1-yl) and Silver(I)

James R. Gardinier
*Marquette University*, james.gardinier@marquette.edu

Jeewantha S. Hewage
*Marquette University*, jeewantha.hewage@marquette.edu

Justin Hoffman
*Marquette University*

Sergey V. Lindeman
*Marquette University*, sergey.lindeman@marquette.edu

Natalia B. Shustova
*University of South Carolina*

*European Journal of Inorganic Chemistry (Special Issue: The Significance of Scorpionate Ligands 50 Years On (Cluster Issue)*, Vol. 2016, No. 15-16 (June 2016): 2615-2625. DOI. 

# Supramolecular Assembly of Metal-Organic Tubes Constructed from the Ditopic Heteroscorpionate Ligand (4-$NH_2C_6H_4$)$CHpz_2$ (pz = Pyrazol-1-yl) and Silver(I)

James R. Gardinier
Department of Chemistry, Marquette University, Milwaukee, WI
Jeewantha S. Hewage
Department of Chemistry, Marquette University, Milwaukee, WI
Justin Hoffman
Department of Chemistry, Marquette University, Milwaukee, WI
Sergey V. Lindeman
Department of Chemistry, Marquette University, Milwaukee, WI
Derek E. Williams
Department of Chemistry, Marquette University, Milwaukee, WI
Natalia B. Shustova

Department of Chemistry and Biochemistry, University of South Carolina, Columbia, SC

## Abstract

The possibility of constructing tubular metal-organic structures with aid of weak hydrogen-bonding interactions between suitably designed metallacycles was explored. For this purpose, the new heteroditopic ligand (4-$NH_2C_6H_4$)$CHpz_2$ (**L1**) was prepared in good (75 %) yield by a one-pot procedure starting from commercial 4-acetamidobenzaldehyde. The equimolar reactions between **L1** and various silver(I) salts gave the intended 1:1 complexes in which the metallacycles were assembled into tubes. However, the exact nature of the assemblies (including their solvate compositions) varied depending on anion, solvent, and concentration of the original crystallization solution. For the trifluoromethanesulfonate anion, a hexameric structure was observed, whereas cyclic dimers were obtained for other anions. In the case of $PF_6^-$, an unusual, opened-cycle structure with the composition [(**L1**)Ag(μ-**L1**)Ag$(CH_3CN)_2]^{2+}$ was also identified crystallographically. The capacity for desolvated tubular structures to be used for gas adsorption was also investigated.

## Abstract

Silver(I) complexes of a new heteroditopic heteroscorpionate have a proclivity for forming tubular assemblies with the aid of weak charge-assisted hydrogen-bonding interactions.


## Introduction

The preparation of single-walled metal-organic nanotubes is an emerging area of research interest**1** because of alluring potential applications in gas storage and separation,**2** sensing,**3** catalysis,**4** environmental remediation,**5** or conductive materials technology.**6** Even though the fabrication of such architectures is fraught with inherent challenges due to the fickle nature of self-assembly,**7** several successful strategies have been employed to produce

tubular systems.**2**-**6**, **8**-**10** One promising strategy is to decorate metallacycles with groups capable of participating in hydrogen-bonding interactions (either charge-assisted or not) to enforce cofacial stacking of rings.**10** Such a strategy is undoubtedly inspired by the success in constructing purely organic rings into nanotubes.**11**

Heteroditopic bis(pyrazolyl)methanes (pyrazolyl = pz) with secondary Lewis donors bound to the methine group are ligands with a proclivity for forming metallacycles and, thus, are of potential interest for assembling into tubes. Manzano's 4-pyridyl derivatives $L^{(*)py}$ (top left, Scheme **1**) readily form cyclic dimeric structures (bottom middle, Scheme **1**) with a variety of metals.**12** Especially noteworthy is $[Ag(L^{*py})](PF_6)\cdot 0.125\ THF\cdot 0.125\ CH_2Cl_2$, which was shown to crystallize with a polymeric (bottom left, Scheme **1**) helical tube structure. The tube was reinforced by charge-assisted weak CH···F hydrogen-bonding interactions to incarcerate $CH_2Cl_2$ solvate molecules. Marchiò's remarkable $L^{(*)SPh}$ ligands with a bis[3,5-(R = H or Me)$_2$pyrazolyl]methyl group attached to diarylthioethers form the gamut of polymeric and cyclic structures with silver(I), depending either on the anion or on the other groups on the aryl thioether.**13** Importantly, derivatives that formed hexameric metallacycles packed to give crystals with permanent micropososity and exhibited reversible, selective adsorption of $CO_2$ (or $N_2O$) over $CH_4$ and $N_2$. Carrano's $L^{*(m\text{- or }p\text{-})CO_2H}$ ligands in which the carboxylic acid (or deprotonated carboxylate) is oriented either *meta* or *para* to the bis(3,5-dimethylpyrazolyl)methyl group (3,5-dimethylpyrazolyl = pz*) formed either polymeric or cyclic dimer structures depending on the metal.**14** It was noteworthy that by changing the protonation state from double to single in silver(I) complexes {i.e., $Ag[L^{*pCO_2H}]_2(ClO_4)$ vs. $Ag(L^{*pCO_2H})(L^{*pCO_2})$} the H-bonded supramolecular structures were tuned from a 1D polymer to a cyclic trimer with a 5–6 Å aperture in the center that holds solvate molecules. Our group recently described silver(I) complexes of the three $L^{P(p\text{-tolyl})}$ isomers (top right, Scheme **1**).**15** When the diarylphosphine group was *ortho*- to the bis(pyrazolyl)methyl group, a coordination polymer was formed, but cyclic dimers were observed in the solid state for *meta* or *para* isomers. $^{31}P$ NMR studies showed that these dimers persisted in solution. Thus, because metal complexes of heteroditopic heteroscorpionates formed a host of metallacyclic structures with interesting properties, we began to focus on modifications of these and other new systems that contain hydrogen-bonding groups to direct their assembly into tubular structures. Here we disclose our first fruitful efforts in this direction, introducing the new ligand $(4\text{-}H_2NC_6H_4)CHpz_2$ (**L1**), detailing its reactions with AgX [X = $BF_4$, $PF_6$, $OSO_2CF_3$ (= OTf), and $NO_3$], and describing seven structures of the resulting complexes.

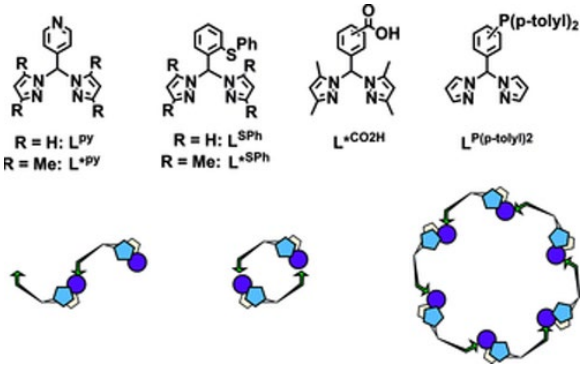


**Scheme 1** Some heteroditopic heteroscorpionate ligands (top) and a sampling of supramolecular isomers formed after metal coordination (bottom).

# Results and Discussion

## Synthesis

The new ligand (4-$H_2NC_6H_4$)$CHpz_2$ (**L1**) was prepared by two different routes, as summarized in Scheme **2**. Of the two pathways, Method A (Scheme **2**, top) is preferred, because a 75 % yield can be obtained after a one-pot, two-step reaction sequence starting from commercial and inexpensive reagents. The yield of the $CoCl_2$-catalyzed Peterson rearrangement**16** between the aldehyde and $S(O)pz_2$ was improved by 10–20 % by using an excess of $S(O)pz_2$ (relative to cases in which a 1:1 stoichiometric ratio of reagents was used). It is also noted that the rate of hydrolysis of the intermediate, {4-[$CH_3C(O)NH$]$C_6H_4$}$CHpz_2$, is greatly enhanced in aqueous solution with respect to in solvent mixtures (THF/water or methanol/water). That is, after monitoring of the amide deprotection reaction by TLC, the rate of hydrolysis was observed to increase with water content of the solvent mixture. The deprotection reaction did not proceed to any appreciable extent when mixtures of NaOH (or KOH) and the intermediate were heated at reflux in dry MeOH over the course of a day, but the reaction was complete within hours when only water was used as a solvent. The ligand has significant solubility in water and in basic solution; this slightly complicates its extraction into organic solvents. That is, yields can be artificially low if care is not taken to ensure complete extraction by using numerous aliquots of organic solvent (ethyl acetate was particularly effective) and by checking the aqueous layer for product by TLC.

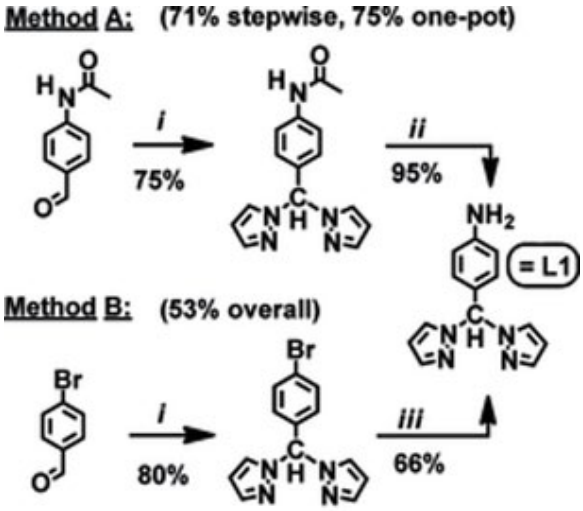


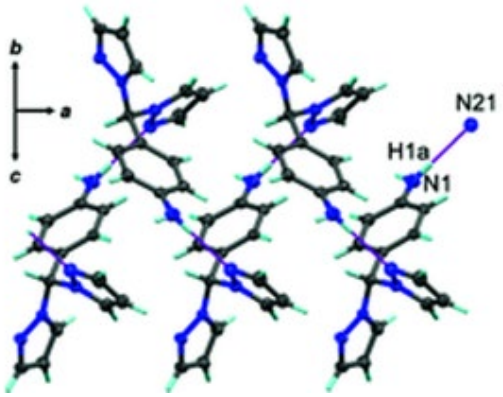

**Scheme 2** Synthesis of ligand **L1** (top) and a portion of its crystal structure (bottom) showing a polymeric chain held together by weak N–H···N hydrogen-bonding interactions [pink lines, H1a···N21 2.19(2) Å]. Key: *i*) 3 S(O)$pz_2$, cat. $CoCl_2$, THF, Δ, 12 h; *ii*) NaOH (ca. 1 m, aq), Δ, 3 h; *iii*) 6 $NH_4OH$ (aq), $Cs_2CO_3$, $Cu_2O$, H(tmhd), DMF, Δ, 15 h.

The second route, Method B (Scheme **2**, middle) employed copper-catalyzed amination between an aryl halide precursor and aqueous ammonia. This route consistently afforded lower yields of product and was less reliable than Method A (because yields varied unpredictably between 40 to 66 %; see Electronic Supporting Information); however, it may be useful for the design of ligand variants where the amide is not available.

Ligand **L1** is soluble in most organic solvents except the lighter alkanes. Single crystals suitable for X-ray diffraction can be grown by diffusion of pentane into $Et_2O$ solutions. As shown at the bottom of Scheme **2** and as fully detailed in the Supporting Information, the three-dimensional packing is dominated by various weak hydrogen-bonding interactions involving the $NH_2$ group and pyrazolyl nitrogen atoms. This packing may be noteworthy, because over the course of months under atmospheric conditions, solid samples of **L1** slowly decomposed with release of pyrazole and became darker yellow to yellow-orange, similar in appearance to the decomposition product of *p*-[CH(O)]$C_6H_4NH_2$ (but the decomposition of this latter species is several orders of magnitude faster than that of **L1**).**17** Thus, the ligand is best stored in a freezer; otherwise it should be purified by recrystallization prior to use after prolonged storage at room temperature. As far as we are aware, **L1** represents only the second example of a bis(pyrazolyl)methyl that decorates an aniline; the first was Manzano's (2-$NH_2C_6H_4$)CHpz*$_2$.**18** The related compounds (2- or 4-$NH_2C_6H_4$)C$pz_3$**19** and (4-$NH_2C_6H_4$)$CH_2$pz**20** are also known.

After mixing THF solutions of **L1** and an equimolar amount of a silver(I) salt, [Ag**L**](X) {X = $BF_4$ (**1**), $PF_6$ (**2**), OTf (**4**), and $NO_3$ (**5**)} precipitated. Each analytically pure solid was obtained in very good yield after the resulting suspension had been filtered, washed with $Et_2O$, and dried under vacuum at 80 °C. The silver complexes are pale yellow and, as solids, appear to be indefinitely stable towards decomposition by light or by self-condensation under ambient conditions. The nitrate **5** is noticeably hygroscopic. As detailed later in the "Solution" section, complexes **1** and **2** each react slowly with acetone in solution to give [Ag($Me_2C$=$NC_6H_4CHpz_2$)](X) {**3**(X), (X = $BF_4$, $PF_6$)}; **4** and **5** are unreactive toward acetone.

## Solid-State Structures

Layering $Et_2O$ onto $CH_3CN$ containing **1** gave crystals of a solvate **1**·0.25 $CH_3CN$. Various views of the structure of **1**·0.25 $CH_3CN$ are given in Figure **1**. The complex crystalizes with a dimeric $[Ag_2\mathbf{L}_2]^{2+}$ dication, with bridging ligands separating the two silver centers by 6.30 Å, precluding any intermetallic interactions. In the dication, each silver is bound to the chelating bis(pyrazolyl)methane "head" of one ligand and to the aniline $NH_2$ "tail" of the second ligand to give a minimum $AgN^{pz}{}_2N^{Ar}$ coordination environment. The two silver centers differ from one another in their relative proximity to the solvate $CH_3CN$ molecule. The Ag1 center is far removed from the solvate molecule and is strictly three-coordinate, whereas there is ambiguity in the coordination number of Ag2. That is, the average Ag1–$N^{pz}$ bond length of 2.28 Å falls within the 2.2–2.3 Å range found for other three-coordinate silver-pyrazolyl compounds.**21** Moreover, the sum of the angles about Ag1 is 360°, with the

three N–Ag1–N angles of 140, 132, and 88° corresponding to an "extended Y" geometry ($\gamma$ < 120° and 120° < $\alpha$, $\beta$ < 180°, where $\alpha$, $\beta$, and $\gamma$ are the largest, middle, and smallest internuclear angles, respectively).**22** On the other hand, the average Ag2–$N^{pz}$ bond length of 2.32 Å falls at the low end of the 2.3–2.4 Å range found for tetracoordinate silver-pyrazolyl compounds and the sum of angles about Ag2 is 356°, which may suggest tetracoordination. However, the 50 % occupancy of the solvate over two nearby sites (related by $C_2$ rotation axes that are parallel to the *b* axis and that exchange molecules shown in pink and yellow, left center of Figure **1**) and the exceptionally long Ag–N1s separation of 2.68 Å (see structure of **2**·$CH_3CN$, below, for comparison) are suggestive of only a weak secondary interaction rather than a strong bond, which gives rise to the ambiguity in coordination number. If Ag2 is three-coordinate, the angles about silver ($\alpha$ = 159°, $\beta$ = 112°, $\gamma$ = 85°) indicate a slightly pyramidal version of a "compressed Y" (120° < $\alpha$ < 180° and 90° < $\beta$, $\gamma$ < 120°) geometry. If Ag2 is tetracoordinate, then the geometry about silver can be considered a "sawhorse" ($\tau_\delta$ = 0.404) according to Kubiak's**23** modification of Houser's**24** $\tau_4$ index. As indicated in the bottom right of Figure **1** and more fully detailed in the Supporting Information, the cyclic dications are organized into tubular structures that run parallel to the *a* axis by a host of short charge-assisted N–H···F weak hydrogen-bonding interactions**25** involving the aniline $NH_2$ groups and tetrafluoroborate anions. Two dications are stacked together to form a dimer that encapsulates the disordered acetonitrile solvate. The interdimer stacking is such that the long axes of neighboring dications are twisted by 74° relative to one another. There are small voids between the contact surfaces of the ions in the crystal lattice that occur parallel to the *a* axis both in the tubes (between every two dications) and between anions (bottom right, Figure **1**) that account for 1.5 % of the unit cell volume (49 $Å^3$, 1.1 Å probe radius, 0.3 Å grid spacing). Attempts to desolvate single crystals while concomitantly monitoring changes in structure by X-ray diffraction were thwarted by cracking during heating and evacuation. An examination of the space-filling model of **1**·0.25 $CH_3CN$ (bottom left, Figure **1**) indicated that acetonitrile nested snugly in the container formed by two dications. This observation also suggested that bulker organonitriles or other larger Lewis donors would not fit into the tubes, so we explored the effects of using other crystallization solvents.

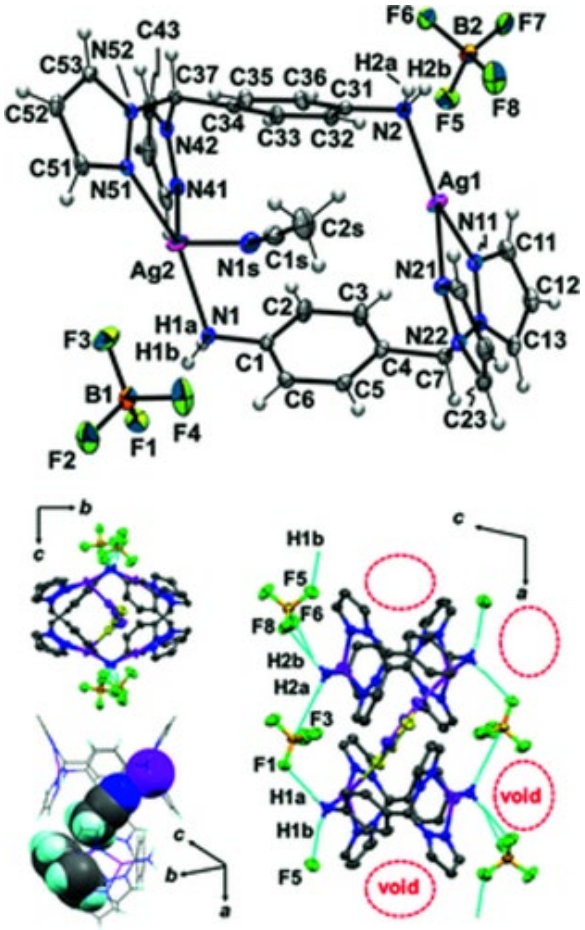


**Figure 1** Views of the structure of **1**·0.25 $CH_3CN$. Top: Thermal ellipsoid plot (drawn at 30 % probability) of asymmetric unit. Bottom: Views of two neighbouring dications held together along the *a* axis by weak NH···F hydrogen-bonding interactions. Selected interatomic distances [Å]: Ag1–N2 2.198(3), Ag1–N11 2.290(3), Ag1–N21 2.263(3), Ag2–N1 2.240(3), Ag2–N41 2.414(3), Ag2–N51 2.224(3), Ag2–N1s 2.676(6). Selected interatomic angles (°): N2–Ag1–N11 131.62(9), N2–Ag1–N21 140.31(9), N21–Ag1–N11 87.82(9), N1–Ag2–N41 112.20(9), N1–Ag2–N1s 85.73(15), N41–Ag2–N1s 131.33(16), N51–Ag2–N1 159.43(9), N51–Ag2–N41 84.68(9), N51–Ag2–N1s 91.69(15).

Gratifyingly, solvate-free **1** crystallized after $Et_2O$ diffusion into a benzonitrile solution (see Figures **2** and **3**). Firstly, it is noted that **1**·0.25 $CH_3CN$ and solvate-free **1** crystallized in different crystal systems: the former is monoclinic (*P*2/*n*) and the latter is orthorhombic (*Pccn*), which explains the difficulty in monitoring desolvation process by single-crystal X-ray diffraction. In **1**, the two silver centers are distinctly three-coordinate even though they have a rather long average Ag–$N^{pz}$ distance of 2.305 Å that is at the borderline of distance ranges for three-/four-coordinate structures; the next nearest contact to silver is with a remote 4-pyrazolyl carbon (Ag1···C12 3.17 Å). The three N–Ag–N angles of 160, 114, and 86° also indicate a planar (Σ[ang] 360°) "compressed Y" geometry about the metal consistent with tricoordination.**22** The dimeric ring structure is preserved in **1** but there are subtle differences in geometry relative to **1**·0.25 $CH_3CN$. As shown in Figure **3**, the metallacycles can be simplified visually by considering six-membered rings consisting of $Ag_2(N_{amino})_2(C_{methine})_2$ atoms. These rings adopt a boat conformation in **1** and **1**·0.25 $CH_3CN$, with the latter being closer to a half-boat. The silver···silver separation is 0.123 Å longer in the former (Ag···Ag 6.423 Å) than in **1**·0.25 $CH_3CN$ (Ag···Ag

6.300 Å). The longer Ag···Ag separation in **1** arises in part from the compression of the phenyl rings of the bridging ligands toward the center of the metallacycle [(Ct = centroid)···Ct distance 4.895 Å in **1** vs. 5.386 Å in **1**·0.25 $CH_3CN$] and a larger slipping of phenyl rings, measured indirectly by the more acute $N_{amino}$–$C_{methine}$–$N_{amino}$ angle of the metallacycle (N1–C7–N1′ 70° in **1**, N1–C7–N2 or N2–C37–N1 = 77° in **1**·0.25 $CH_3CN$). Moreover, despite having two different compositions and crystal systems, the supramolecular tube structure and crystal packing of **1** and **1**·0.25 $CH_3CN$ are remarkably similar (for full details see the Supporting Information). Figure **4** shows views of the crystal packing of **1** with small void spaces (purple globular objects) between contact surfaces of ions (74.6 $Å^3$, 2.4 % of unit cell; 1.1 Å probe radius, 0.3 Å grid spacing). Similarly to in **1**·0.25 $CH_3CN$, charge-assisted weak hydrogen-bonding interactions between the tetrafluoroborate anion and the $NH_2$ groups (N1H1a···F4 2.08 Å, 167°; N1H1b···F3 2.10 Å, 164°) assemble the dications (with 69° twist between neighboring rings) into tubes that runs parallel with the *c* axis. The dications are evenly spaced 6.253 Å apart [measured between centroids of six-member $Ag_2(N_{amino})_2(C_{methine})_2$ rings, $Ct^{cycle}$···$Ct^{cycle}$] in **1** whereas the rings are further and alternately spaced (intra- and interdimer $Ct^{cycle}$···$Ct^{cycle}$ 6.633 and 6.682 Å, respectively) in **1**·0.25 $CH_3CN$. Thus, the hydrogen-bonding interactions and flexible metallacycle framework provide compression/expansion capacity to the tubular structures.

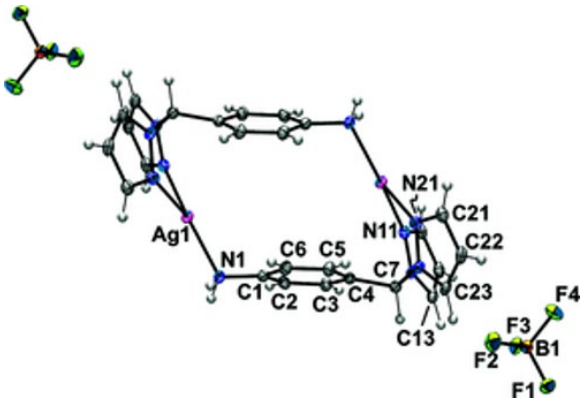


**Figure 2** View of **1**, approximately down the crystallographic twofold axis (thermal ellipsoids at 30 % probability level). Selected interatomic distances [Å]: Ag1–N1 2.186(3), Ag1–N11 2.192(3), Ag1–N21 2.418(3). Selected interatomic angles [°]: N1–Ag1–N11 160.20(10), N1–Ag1–N21 114.23(10), N11–Ag1–N21 85.54(10).

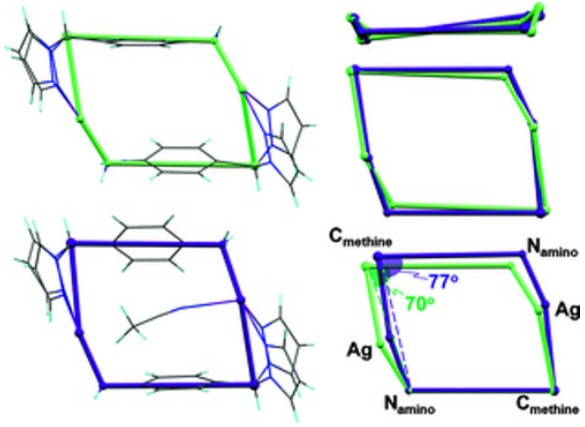


**Figure 3** Left: Simplified six-member representations of cyclic dications in the structures of **1** (pale green, top) and **1**·0.25 $CH_3CN$ (violet, bottom). Right: Views of representations overlayed by minimizing distances between similar sets of six atoms (top two views, rmsd 0.272) or of two atoms (one $N_{amino}$ and $C_{methine}$, bottom) on each ring.

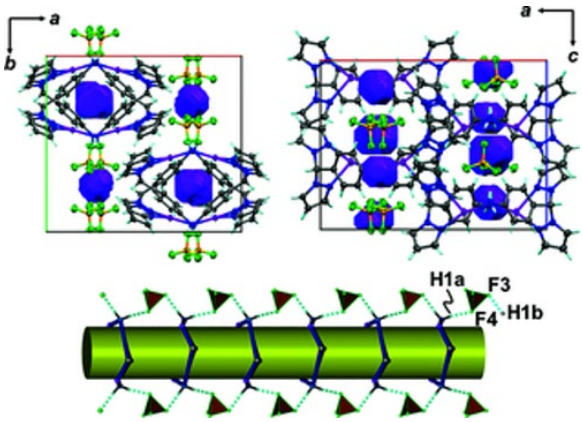

**Figure 4** Views of the crystal packing and tubular structure of **1**.

Crystallization of **2** by $Et_2O$ vapor diffusion into $CH_3CN$ solutions produced two different types of crystals depending on the concentration of the initial solution. When $CH_3CN$ solutions are 0.04 m (or greater) in **2**, colorless prism/needles of **2**·0.125 $CH_3CN$ are obtained. When $CH_3CN$ solutions are 0.02 m (or less) in **2**, colorless feather-like plates of **2**·$CH_3CN$ are obtained; mixtures of crystals are obtained from 0.03 m solutions of **2**. As shown and described more fully in the Supporting Information, the structure of **2**·0.125 $CH_3CN$ resembles that of **1**, with metallacyclic dications stacked into tubes along the crystallographic *c* axis (*P*1 space group) but the charge-assisted weak hydrogen-bond interactions occur between $NH_2$ groups and hexafluorophosphate anions. It is noteworthy that there are two types of metallacycles, alternately stacked, but evenly spaced ($Ct^{cycle}\cdots Ct^{cycle}$ 6.564 Å, 72° rotation) along the *c* axis: those without and those with partially occupied disordered solvate molecules. Both types of metallacycles have planar six-membered $Ag_2(N_{amino})_2(C_{methine})_2$ rings (sum of internal angles: 720°). The silver centers in each dication are planar (Σ[ang] about each Ag: 360°) with three-coordinate "extended Y" geometries. Thus, the rather long Ag–N1s separation of 2.66 Å in the partially filled metallacycles is probably best considered a secondary interaction rather than a strong bonding interaction.

The crystal structure of the feather-like plates of the full solvate **2**·$CH_3CN$ is strikingly different from that of **2**·0.125 $CH_3CN$ or those of **1** in that the bimetallic dication is not cyclic, but has a remarkable open-cycle structure (Figure **5**). That is, the dication is made up of two silver centers, two heterscorpionate ligands, and two bound acetonitrile ligands. One silver center – Ag1 – is planar three-coordinate with a distorted "orthogonal Y" geometry (i.e., *α/β/γ* close to 150°/120°/90°) and is bound to the chelating pyrazolyl nitrogen atoms of a terminal heteroscorpionate ligand (Ag–$N^{pz}$ avg. 2.28 Å) and to the amino nitrogen of a bridging heteroscorpionate. The four-coordinate silver center – Ag2 – has a distorted sawhorse geometry ($\tau_d$ = 0.59) as a result of binding to the chelating end of the bridging heteroscorpionate (Ag–$N^{pz}$ avg. 2.37 Å) and to two acetonitrile nitrogen atoms (avg. Ag–N: 2.31 Å). The "S-" conformation of the open-cycle dication is not supported by any "intramolecular" hydrogen-bonding interaction (the C37H37···N1 distance of 2.84 Å is too remote and the associated 123° angle is too acute). Rather, the dication and the overall three-dimensional supramolecular structure are stabilized by "intermolecular" charge-assisted hydrogen-bonding interactions involving the amino hydrogen atoms and $PF_6$ anions, as detailed in the Supporting Information.

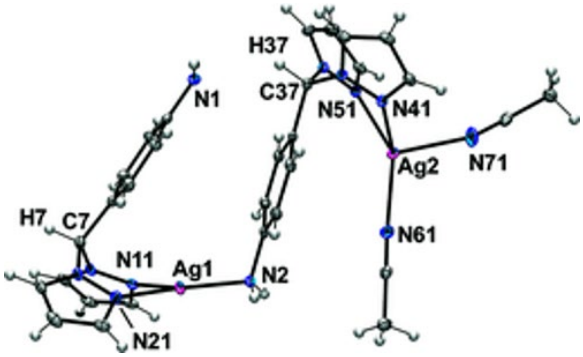


**Figure 5** The structure of the dication in **2**·$CH_3CN$ with partial atom labeling. Thermal ellipsoids drawn at 30 % probability level. Selected interatomic distances [Å]: Ag1–N2 2.1884(18), Ag1–N11 2.2293(18), Ag1–N21 2.3340(18), Ag2–N41 2.4042(18), Ag2–N51 2.3454(18), Ag2–N61 2.2505(19), Ag2–N71 2.375(2). Selected interatomic angles [°]: N2–Ag1–N11 148.05(8), N2–Ag1–N21 126.00(8), N11–Ag1–N21 85.67(6), N51–Ag2–N41 81.12(6), N51–Ag2–N71 111.74(8), N61–Ag2–N41 112.26(7), N61–Ag2–N51 142.29(7), N61–Ag2–N71 104.19(8), N71–Ag2–N41 87.39(7).

When the crystallization solvent system is changed to acetone/hexane, **2** reacts by condensation to give crystalline [Ag**L2**]($PF_6$) (**L2** = $Me_2C{=}NC_6H_4CHpz_2$), **3**($PF_6$). The nature of this reaction is detailed later, in the solution section. Figure **6** provides the structure of the dication in **3**($PF_6$). The bimetallic dication is a cyclic dimer that has inversion symmetry. Each silver is planar (Σ[ang] = 360°) three-coordinate with an extended Y geometry as a result of binding to the chelate end (Ag–$N^{pz}$ avg. 2.28 Å) of one ligand and the imino end (N1–C8 1.255 Å is a characteristic C=N double bond length) of the second bridging ligand [Ag–N1: 2.170(4) Å]. As such, the Ag···Ag distance of 6.374 Å is intermediate between those in the other metallacycles discussed above. The six-membered $Ag_2(N_{imino})_2(C_{methine})_2$ ring is nearly planar (sum of internal angels: 716°) with a slight deformation to give a chair conformation with silver centers at the head and foot. Despite the rings being of similar size to those in **1** or **2**·0.125 $CH_3CN$, the lack of structure-directing $NH_2$ groups alters the crystal packing such that tubes are not formed. Instead, the predominant noncovalent interactions that organize the three-dimensional supramolecular structure are charge-assisted CH···F interactions**26** and a π–π**27** interaction (see the Supporting Information for more details). These interactions are such that neighboring pyrazolyl rings occupy spaces above and below metallacyclic rings, resulting in completely efficient packing.

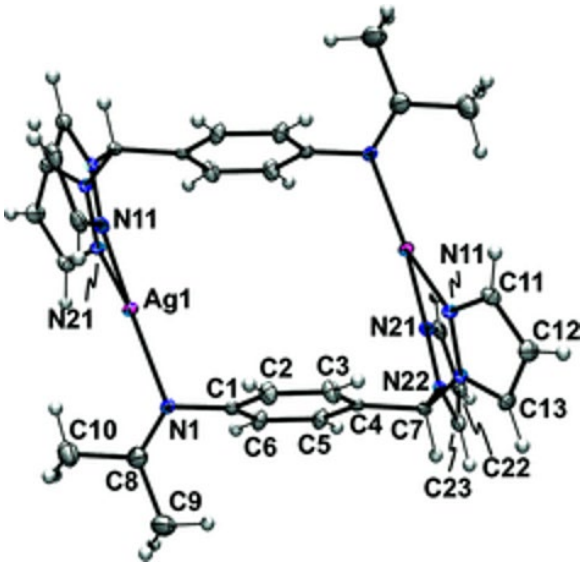


**Figure 6** The structure of the dication in **3**($PF_6$). Thermal ellipsoids drawn at 30 % probability level. Selected interatomic distances [Å]: Ag1–N1 2.170(4), Ag1–N11 2.318(4), Ag1 N21 2.246(4). Selected interatomic angles [°]: N1–Ag1–N11 129.07(14), N1–Ag1–N21 144.61(15), N21–Ag1–N11 86.27(14).

In contrast with either **1** or **2**, crystallization of **4** from any of a variety of solvent systems (for example, $CH_3CN/Et_2O$ or acetone/hexanes) or different concentration ranges only leads to the same type of crystal. Figure **7** shows the asymmetric unit, and Figures **8** and **9** give different views of the extended structure. Complex **4** crystallizes with a body-centered cubic packing arrangement (space group *Ia*3). The overall unit cell contains 48 units of Ag(**L1**)(OTf).

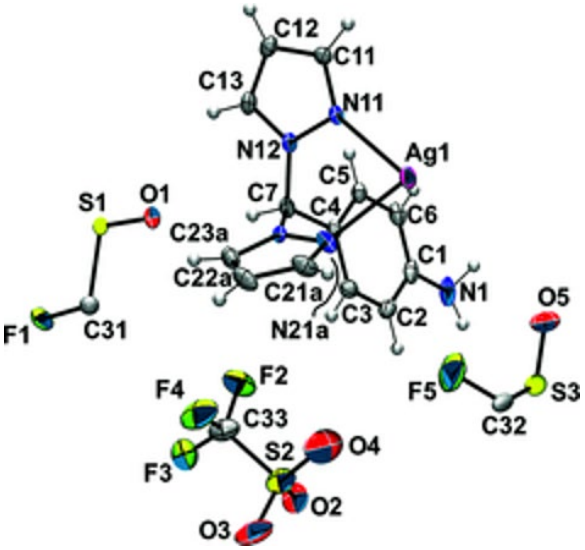


**Figure 7** Major disorder component (57 %, with pyrazolyl ring containing N21a shown) of the asymmetric unit of **4**. Selected interatomic distances [Å]: Ag1–N1 2.257(4), Ag1–N11 2.274(3), Ag1–N21a 2.473(13). Selected interatomic angles [°]: N1–Ag1–N11 152.46(14), N1–Ag1–N21a 118.5(10), N11–Ag1–N21a 81.6(7).

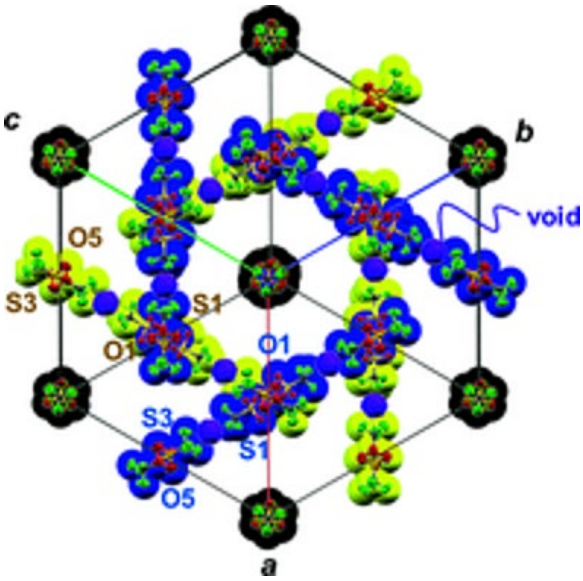


**Figure 8** View of unit cell showing the two types of triflate anions (containing S1 and S3) and voids (purple globular objects) located on threefold rotoinversion axes. The space-filling models are differently coloured for perspective.

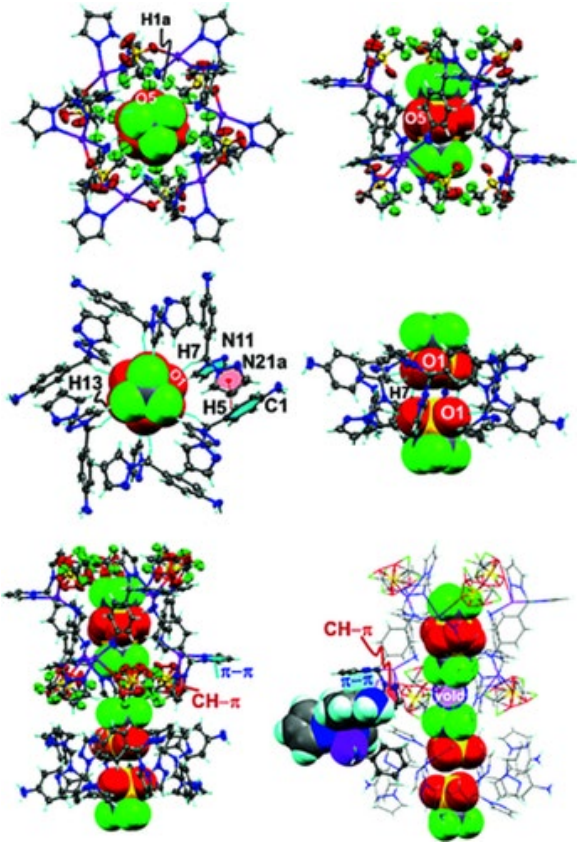


**Figure 9** Top: Views of hexamer A $\{[Ag_6(\mathbf{L1})_6(OTf)_4]^{2+}\}$. Middle: Views of hexamer B $\{[(\mathbf{L1})_6(OTf)_2]^{2-}\}$ with atoms or rings involved in noncovalent interactions labeled. Bottom left: Stacking of hexamers to form tubes with view of noncovalent interaction holding different tubes together. Bottom right: Alternative view emphasizing CH–π and π–π interactions between one tube and an Ag(**L1**) fragment of another tube.

There are three types of triflate anion in the unit cell; their identities are established first in order to facilitate the description of the complicated three-dimensional structure of **4**. Two types of triflate

(OTf-*I* and -*II*) are not bound to silver, whereas the third (OTf-*III*) is bound. OTf-*I* and -*II* are located at special positions (Wyckoff 16c) with their corresponding S1–C31 and S3–C32 bonds on threefold rotoinversion axes and the inversion center located at or below the mean plane of the three oxygen atoms bound to sulfur (O1 and O5, respectively). The atoms of OTf-*I* (with S1) are singly occupied whereas those of OTf-*II* (with S3) are half-occupied. As such, these triflate anions are either located (OTf-*I*) or disordered (OTf-*II*) over two nearby positions with different distances between sulfur centers: S1···S1 = 4.216 Å and S3···S3 = 1.207 Å. Figure **8** shows the arrangement of the channels containing these two types of triflate anions that are coincident with the threefold rotoinversion axes. There are small voids in the contact space between the $CF_3$ groups of these alternately stacked pairs of triflate anions (purple globular objects in Figure **8**) that only account for 87.32 $Å^3$, or 0.4 % of the unit cell volume (1.1 Å probe radius, 0.3 Å grid spacing). The third type of triflate, with half-occupancy, has its S2–O2 bond residing close to, but not on, a twofold axis so it is disordered over two nearby positions. The OTf-*III* is in close contact with silver and is held to the metal either through a strong secondary ion–dipole interaction or through a very weak bonding interaction, because the Ag1···O2 2.67 Å distance is longer than the average distance (2.48 ± 0.13 Å) but is within the ca. 2.25–2.75 Å range found for silver(I)–O(triflate) bonding interactions.**15** The average Ag–$N^{pz}$ distance [2.37 Å (major disorder component), 2.27 Å (minor component), or 2.33 Å (overall)] is at the borderline between three- and four-coordinate silver.

The three-dimensional coordination network structure can be described in terms of alternate stacking of two types of hexameric rings that form the OTf-*I*/OTf-*II* ion channels. These hexameric rings have the nominal compositions $[Ag_6(\mathbf{L1})_6(\text{OTf-}II)_4]^{2+}$ (hexamer A) and $[(\mathbf{L1})_6(\text{OTf-}I)_2]^{2-}$ (hexamer B). If one at first disregards the triflate ions, then hexamer A is constructed from six [Ag(μ-κ$^2$*N*,κ$^1$*N*-**L1**)]$^+$ units arranged in a head-to-tail manner to give a saddle-shaped metallacycle with $S_6$ point group symmetry. The inclusion of six half-occupied type-*III* triflate anions serves to decorate the rim and fill the walls of a cylinder. The resulting cylinder encapsulates an OTf-*II* ion that is disordered over two positions, with $SO_3$ groups oriented either “up” or “down” (Figure **9**, top). The OTf-*II* ion is held in the center of the metallacycle cavity by weak NH···O hydrogen-bonding interactions (N1H1a···O5 2.170 Å, 127°).**28** Overall, the cylinder has a height of 1.5 nm (Ct···Ct distance between the three most remote H22a atoms decorating the top and bottom of hexamer A) and an inner diameter of 0.43 nm (≈ diameter of a triflate ion = diameter of the circumcircle of the triangle of three O5 atoms plus the van der Waals diameter of oxygen). Hexamer B has two well-ordered type-I triflate ions that sandwich six ligands to give a wheel with $S_6$ point group symmetry, as in the middle of Figure **9**. Two CH···O interactions**29** and a concerted set of CH–π**30** and π–π**27** interactions involving an aryl and two pyrazolyl rings (an aryl-pyrazolyl embrace)**31** hold the wheel together. The acidic methine hydrogen H7 interacts with O1 of one triflate (C7H7···O1 2.49 Å, 155°) whereas the 5-pyrazolyl hydrogen – H13 – on the same ligand further supports the structure by more weakly interacting with O1 of the other triflate (C7H7···O1 2.54 Å, 131°). By symmetry, then, each O1 is involved in a bifurcated weak hydrogen-bonding interaction with two neighboring ligands of hexamer B. The aryl ring of the aniline group (with atom C1) is involved in a slipped π–π interaction with the pyrazolyl ring containing N11 [Ct(C1)···Ct(N11) 3.629(2) Å, $\alpha$ = dihedral between planes = 4°, $\beta$ = slip angle = 23°, $\gamma$ = slip angle orthogonal to $\beta$ = 20°] and also serves as a donor in a CH–π interaction with a pyrazolyl acceptor that contains N21a [C5H5···Ct(N21a) 2.74 Å, 133°]. Hexamers A and B are stacked alternately on top of each

other along the threefold rotoinversion axes, as indicated earlier. It is worth reiterating that this structural description is only a simplification: the ligands of hexamer B, in fact, each serve as one part of the wall of a hexamer A in an adjacent tube by binding silver atoms with their nitrogen atoms.

Finally, many attempts were made to grow crystals of **5** for single-crystal X-ray diffraction, but only poorly diffracting triplet crystals were obtained. The diffraction data were sufficient to allow connectivity information to be obtained, but few other meaningful data could be extracted. Of note is that the structure contains cyclic dimers arranged into a tubular array similar to **1**, **1**·0.25 $CH_3CN$, or **2**·0.125 $CH_3CN$ (see Figure S12 in the Supporting Information).

## IR Spectra

The amino $NH_2$ groups each give two characteristic N–H stretches in the 3500–3300 $cm^{-1}$ region of the IR spectrum. These bands occurred at $\nu_{NH}$ 3464 and 3331 $cm^{-1}$ in the spectrum of solid **L1** for asymmetric and symmetric stretching modes, respectively. On complexation the two bands shifted to lower energy in relation to those of the free ligand. Moreover, within the series of desolvated complexes **1**–**4**, the bands showed a shift to lower energy and became broader with increasing coordination capabilities and expected strength of NH···X (X = O, F) hydrogen-bonding interactions of the ions (e.g., with the Hofmeister series**32**) in the order: $PF_6^-$ (highest energy, narrowest band) > $BF_4^-$ > $OTf^-$ > $NO_3^-$ (lowest energy, broadest band).

## Thermal Stability/PXRD/Gas Adsorption

In view of the imperfect crystal packing in **1** and **1**·0.25 $CH_3CN$, the ease of desolvation, the expected weakness of NH···X hydrogen bonds, and the low coordination number of silver(I) that could potentially bind to unsaturated guest molecules, we investigated whether or not **1** or **1**·0.25 $CH_3CN$ would possess enough structural flexibility to exhibit any useful gas sorption properties. These complexes were stable up to about 180–200 °C by TGA analyses (Figure S9 in the Supporting Information). A further increase in temperature caused sample decomposition, verified by visual inspection of samples and in agreement with melting point determinations. On the basis of the TGA data, the evacuation procedure of the prepared samples was performed at 100–160 °C for 1–3 days. The sample integrity before and after evacuation was monitored by PXRD analysis. Unfortunately, none of the samples exhibited any gas absorption properties. Despite the fact that **1** and **1**·0.25 $CH_3CN$ maintain their crystallinity (Figures S10–12 in the Supporting Information) after the evacuation procedure and gas sorption analysis, no $N_2$ uptake was observed. For **1**, the $CO_2$ adsorption isotherm was also collected, but the sample did not exhibit noticeable $CO_2$ uptake. Increases either in the evacuation time, from 24 h to 3 days, or in the temperature did not result in any changes in the sample adsorption properties. A sample of **5** showed complete loss of crystallinity during the evacuation, so gas sorption analysis was not performed. Ultimately, the structures were neither porous enough nor flexible enough in the solid state to provide solvent-accessible void space.

## Solution

NMR spectroscopic and ESI(+) mass spectrometric measurements showed that the solid-state structures of **1**–**5** were disassembled in solution. The different chemical shifts of the hydrogen atoms of the ligand in each of the complexes or in the absence of silver indicate that the ligand is indeed bound to silver in solution. However, the number of resonances was fewer than would be expected for static

structures that resembled the species characterized in the solid state. Particularly informative is the fact that identical NMR spectra were obtained for solutions when crystals of either **2**·0.125 $CH_3CN$ (cyclic) or **2**·$CH_3CN$ (opened cycle) were dissolved in $CD_3CN$. If the solid-state structures were maintained, the latter sample should show twice the number of resonances as the first; there was no apparent change in the spectra on lowering the temperature to 243 K, just above the freezing point of the solvent. Moreover, the ESI(+) mass spectra of samples indicate that extensive dissociation occurs in $CH_3CN$ solution. The solid-state structure of **4** had the highest dimensionality of the complexes here (hexameric rings), yet the ESI(+) mass spectrum only showed peaks at m/*z* 585 for $[Ag(\mathbf{L1})_2]^+$ (100 %), 517 for $[Ag(\mathbf{L1})(\mathbf{L1\text{-}Hpz})_2]^+$ (12 %), and 387 for $[Ag(\mathbf{L1})(CH_3CN)]^+$ (40 %). No higher-order peaks for $[Ag_n(\mathbf{L1})_m]^{n+}$ ($n > 1$, $m > 2$) fragments nor related species (with varying number of associated triflates) were observed for this or any other of the complexes in this work.

Finally, it was also of interest to ascertain whether the condensation reaction that gave **3**($PF_6$) occurred for complexes of the other anions and under what conditions this reaction occurred. The solubility of the various complexes in [$D_6$]acetone is of the order **2** > **1** >> **4** or **5** (insoluble). This is also the same order in which the complexes undergo condensation reactions in solution. When **2** is dissolved in [$D_6$]acetone, the condensation reaction to form **3**($PF_6$) is essentially complete within 4 h (Figure **10**). The 12:1 ratio of **3**($PF_6$)/**2** obtained (by NMR resonance integration) after 4 h remained unchanged after several days. The similar reaction with **1** to form **3**($BF_4$) was complete after 16 h; **4** and **5** did not react because they were insoluble. When crystals of **3**($PF_6$) were dissolved in wet $CD_3CN$, complete hydrolysis occurred immediately to give **2**, indicating that the sample is sensitive to moisture. The addition of 4 Å molecular sieves to the solution of the hydrolyzed sample caused slow reconversion into **3**($PF_6$) through removal of $H_2O$.

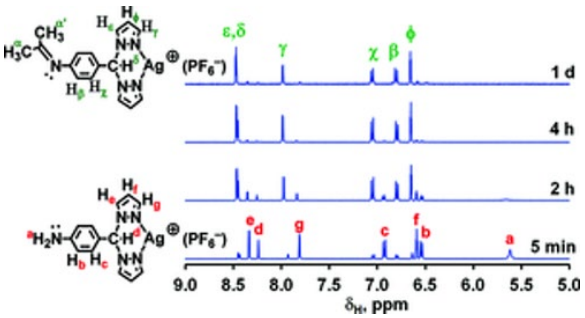


**Figure 10** Downfield portion of room-temperature $^1H$ NMR spectrum acquired at various time intervals after **2** was dissolved in [$D_6$]acetone, showing the formation of **3**($PF_6$) (main signals, top spectrum).

## Conclusions

Heteroscorpionates based on decorating a bis(pyrazolyl)methane with another Lewis donor at the methine "tail" position are reliable platforms for obtaining cyclic architectures on complexation to metals. In this work we showed not only that silver(I) complexes of the new ligand **L1**, with an aniline "tail", give the expected dimeric cyclic structures, but, in addition, that hexameric and oligomeric species can also be obtained under suitable circumstances. More importantly, weak hydrogen-bonding interactions between the $NH_2$ group and anions can direct the formation of tubular structures with somewhat flexible geometries. The effects of increasing spacer or anion size, as well as alternative

modifications of the scorpionate backbone to provide permanent porosity, are currently being pursued.

## Experimental Section

**General Considerations:** Pyrazole, NaH powder, thionyl chloride, anhydrous $CoCl_2$, 4-acetamidobenzaldehyde, 4-bromobenzaldehyde, and all silver salts were purchased commercially and were used as received. THF was distilled under nitrogen from a deep blue sodium benzophenone ketyl solution prior to use.

**Instrumentation:** Midwest MicroLab, LLC, Indianapolis, Indiana 45250, performed elemental analyses. IR spectra were acquired on solid samples with a Thermo Scientific Nicolet iS5 IR spectrometer equipped with an iD3 Attenuated Total Reflection (ATR) accessory. $^{1}H$ (400 MHz) and $^{13}C$ (100.52 MHz) NMR spectra were recorded with a Varian spectrometer. Chemical shifts were referenced to solvent resonances at $\delta_H$ = 7.26, $\delta_C$ = 77.16 ppm for $CDCl_3$, $\delta_H$ = 1.94 and $\delta_C$ = 118.26 ppm for $CD_3CN$, and $\delta_H$ = 2.05, $\delta_C$ = 29.92 ppm for [$D_6$]acetone. Melting-point determinations were made with an Electrothermal 9100 apparatus on samples contained in glass capillaries and are uncorrected. Mass spectrometric measurements recorded in ESI(+) or ESI(–) mode were obtained with a Micromass Q-TOF spectrometer, whereas those performed by direct-probe analyses were made with a VG 70S instrument. For the ESI(+/–) experiments formic acid (approximately 0.1 %, *v/v*) was added to the mobile phase ($CH_3CN$). Powder X-ray diffraction patterns were collected on a zero diffraction plate with a Rigaku Miniflex II diffractometer and an accelerating voltage of 30 kV and a current of 15 mA. The PXRD patterns of the samples were taken before and after evacuation of the samples to confirm sample crystallinity.

A Quantachrome Autosorb 1-C Analyzer was used to measure nitrogen and carbon dioxide adsorption isotherms. Oven-dried quartz sample tubes were cooled from the oven prior to loading of the sample, which was then capped and transported to the instrument outgassing station. Samples were heated to the appropriate temperatures as determined by TGA analysis prior to being weighed and transferred to the sample station for analysis. $N_2$ isotherms were measured with use of a liquid nitrogen bath (77 K). Ultra high purity grade (99.999 % purity) $N_2$, $CO_2$, and He, oil-free valves and gas regulators were used for all free space corrections and measurements.

Thermogravimetric analyses were performed with a SDT Q600 Thermogravimetric Analyzer and an alumina boat sample holder.

### Synthesis

**$H_2NC_6H_4CHpz_2$ (L1):** A one-pot procedure is described below. Descriptions of the stepwise version of this procedure [in which the intermediate $CH_3C(O)NC_6H_4CHpz_2$ is isolated] and an alternative preparative route (the amination of $BrC_6H_4CHpz_2$) are provided in the Supporting Information.

**One-Pot Preparation:** Under argon, a solution of pyrazole (2.50 g, 36.4 mmol) in THF (20 mL) was added slowly by cannula transfer (to control hydrogen evolution) to a suspension of NaH (0.882 g, 36.8 mmol) in THF (30 mL). To ensure quantitative transfer, additional THF (10 mL) was added to the flask that had originally contained the pyrazole, and the washing was transferred to the colorless Napz solution. After the Napz solution had been stirred for 20 min, a solution of $SOCl_2$ (1.33 mL, 2.19 g, 36.4

mmol) in THF (10 mL) was added by cannula [quantitative transfer was ensured by washing the flask originally containing $SOCl_2$ with additional THF (10 mL) and subsequent cannula transfer to the reaction mixture]. After the pale yellow milky THF suspension of $S(O)pz_2$ and NaCl had been stirred for 30 min, $CoCl_2$ (0.159 g, 1.23 mmol) was added in one portion under argon. After the blue suspension had been stirred for 5 min, solid 4-acetamidobenzaldehyde (2.00 g, 12.3 mmol) was added in one portion under argon and the resulting mixture was heated at reflux for 12 h under argon. The suspension changed color from royal blue to bright green in the first hour and was olive green at the end of the reflux period. After the mixture had cooled to room temperature, THF was removed under vacuum. A solution of NaOH (4.92 g, 0.123 mol) in deionized water (150 mL) was added, and the orange mixture was heated at reflux for 3 h (until complete hydrolysis of the amide had occurred, as monitored by TLC, see below), during which time the suspension became dark brown. The product mixture was allowed to cool to room temperature and filtered to remove undesired solid (presumably cobalt hydroxide), and the aqueous solution was extracted with ethyl acetate (five 50 mL portions). The combined organic extracts were dried with $MgSO_4$ and filtered, and solvent was removed by rotary evaporation to leave an orange oil that was loaded onto a silica gel column (h 6'' × diam, 1.5''). Elution of the yellow band with ethyl acetate/hexanes (1:1, *v/v*, $R_f$ 0.4) and removal of solvent under vacuum afforded **L1** (2.20 g, 75 %) as a pale yellow solid, m.p. 118–119 °C. $^1$H NMR ($CDCl_3$): $\delta$ = 7.63 (s, 1 H, $CHpz_2$), 7.62 (d, $J$ = 1.5 Hz, 2 H, $H_3$pz), 7.47 (d, $J$ = 2.4 Hz, 2 H, $H_5$pz), 6.86 (part of *AB*, 2 H, Ar), 6.64 (part of *AB*, 2 H, Ar), 6.31 (dd, $J$ = 2.4, 1.5 Hz, 2 H, $H_4$pz), 3.79 (s, 2 H, $NH_2$) ppm. $^{13}$C NMR ($CDCl_3$): $\delta$ = 147.5 ($C_{1or4}$Ar), 140.8 ($C_5$pz), 129.6 ($C_3$pz), 128.4 ($C_{3,5}$Ar), 125.7 ($C_{4or1}$Ar), 115.1 ($C_{2,6}$Ar), 106.4 ($C_4$pz), 77.9 ($C_{meth}$) ppm. IR (KBr): $\tilde{\nu}_{NH}$ = 3464, 3331, 3213 (N–H bend overtone) cm$^{-1}$. $C_{13}H_{13}N_5$: calcd. (found) C 65.25 (64.97), H 5.48 (5.35), N 29.27 (29.01). Crystals suitable for X-ray diffraction were grown by layering pentane onto a solution of **L1** in $Et_2O$ and allowing solvents to diffuse slowly overnight.

**[Ag(L1)](BF$_4$), 1:** A solution of **L1** (0.212 g, 0.885 mmol) in THF (10 mL) was added to a solution of $Ag(BF_4)$ (0.173 g, 0.885 mmol) in THF (10 mL). After the resulting solution had been stirred at room temperature for 2 h, solvent was removed by cannula filtration. The residue was washed with $Et_2O$ (two 5 mL portions) and dried under vacuum to leave **1** (0.349 g, 91 %) as a colorless solid, m.p. 184–185 °C (decomposed). $^1$H NMR ($CD_3CN$): $\delta$ = 7.91 (dd, $J$ = 2.5, 0.6 Hz, 2 H, $H_5$pz), 7.72 (s, 1 H, CH), 7.59 (d, $J$ = 1.9 Hz, 2 H, $H_3$pz), 6.61 (d, $J$ = 8.7 Hz, 2 H, $H_{2,6}$Ar), 6.47 (dd, $J$ = 8.8, 0.8 Hz, 2 H, $H_{3,5}$Ar), 6.42 (dd, $J$ = 2.5, 1.9 Hz, 2 H, $H_4$pz), 4.38 (s, 2 H, $NH_2$) ppm. $^{13}$C NMR ($CD_3CN$): $\delta$ = 150.0 ($C_{1or4}$Ar), 142.8 ($C_3$pz), 133.2 ($C_5$pz), 128.9 ($C_{3,5}$Ar), 124.2 ($C_{4or1}$Ar), 115.1 ($C_{2,6}$Ar), 107.2 ($C_4$pz), 77.0 ($C_{meth}$) ppm. $^{19}$F NMR ($CD_3CN$): $\delta$ = 151.67, 151.70 ppm. IR (KBr): $\tilde{\nu}_{NH}$ = 3344, 3294 cm$^{-1}$. $C_{13}H_{13}N_5AgBF_4$: calcd. (found) C 35.98 (36.22), H 3.02 (3.14), N 16.14 (16.38). Crystals suitable for X-Ray diffraction were grown by vapor diffusion of $Et_2O$ into a benzonitrile solution of **1**.

**[Ag(L1)(CH$_3$CN)$_{0.25}$](BF$_4$) (1·0.25 CH$_3$CN):** Crystals suitable for X-ray diffraction were grown by vapor diffusion of $Et_2O$ into an acetonitrile solution of **1**.

**[Ag(L1)](PF$_6$) (2):** A solution of 0.195 g (0.817 mmol) **L1** in THF (10 mL) was added to a solution of 0.207 g (0.817 mmol) $Ag(PF_6)$ in THF (10 mL). After the resulting solution had been stirred at room temperature for 2 h, solvent was removed by cannula filtration. The residue was washed with $Et_2O$ (two 5 mL portions) and dried under vacuum to leave **2** (0.364 g, 90 %) as a colorless solid, m.p. 170–171 °C (decomposed). $^1$H NMR ($CD_3CN$): $\delta$ = 7.71 (d, $J$ = 2.5 Hz, 2 H, $H_5$pz), 7.50 (s, 1 H, CH), 7.34 (d, $J$ =

1.6 Hz, 2 H, $H_3$pz), 6.37 (d, *J* = 8.6 Hz, 2 H, Ar), 6.19 (m, 4 H, Ar, pz), 4.15 (s, 2 H, $NH_2$) ppm. $^{13}$C NMR ($CD_3CN$): $\delta$ = 150.0 ($C_{1or4}$Ar), 143.0 ($C_3$pz), 133.5 ($C_5$pz), 128.9 ($C_{3,5}$Ar), 124.1 ($C_{4or1}$Ar), 115.1 ($C_{2,6}$Ar), 107.3 ($C_4$pz), 76.9 ($C_{meth}$) ppm. $^{19}$F NMR ($CD_3CN$): $\delta$ = –72.86 (d, *J* = 705.8 Hz) ppm. IR (KBr): $\tilde{\nu}_{NH}$ = 3370, 3321 cm$^{-1}$. $C_{13}H_{13}N_5AgF_6P$: calcd. (found) C 31.73 (32.00), H 2.66 (2.73), N 14.23 (13.99).

**[Ag(L1)($CH_3CN$)$_{0.125}$]($PF_6$) (2·0.125 $CH_3CN$):** Colorless prisms suitable for X-ray diffraction were grown by vapor diffusion of $Et_2O$ into an acetonitrile solution that was 0.04 m in **2** [**2** (20 mg) in $CH_3CN$ (1 mL)].

**[Ag(L1)($CH_3CN$)]($PF_6$) (2·$CH_3CN$):** Colorless crystalline plates suitable for X-ray diffraction were grown by vapor diffusion of $Et_2O$ into an acetonitrile solution that was 0.02 m in **2** [**2** (10 mg) in $CH_3CN$ (1 mL)].

**[AgL2]($PF_6$), (L2 ≡ $Me_2C$=$NC_6H_4CHpz_2$) [3($PF_6$)]:** Crystalline plates suitable for X-ray diffraction were grown by layering hexanes on an acetone solution of **2** and allowing the solvents to diffuse slowly over 2 d. $^1$H NMR ([$D_6$]acetone): $\delta$ = 8.48 (d, *J* = 3 Hz, 2 H, $H_5$pz), 8.47 (s, 1 H, CH), 7.99 (d, *J* = 2 Hz, 2 H, $H_3$pz), 7.05 (d, *J* = 8.6 Hz, 2 H, Ar), 6.80 (d, *J* = 8.6 Hz, 2 H, Ar), 6.66 (dd, *J* = 3, 2 Hz, 2 H, $H_4$pz), 2.64 (s, 3 H, $CH_3$), 2.01 (s 3 H, $CH_3$) ppm. $^1$H NMR ($CD_3CN$): $\delta$ = 7.98 (d, *J* = 3 Hz, 2 H, $H_5$pz), 7.87 (s, 1 H, CH), 7.64 (d, *J* = 2 Hz, 2 H, $H_3$pz), 6.73 (m, 4 H, Ar), 6.47 (dd, *J* = 3, 2 Hz, 2 H, $H_4$pz), 2.19 (s, 3 H, $CH_3$), 1.77 (s 3 H, $CH_3$) ppm. $^{13}$C NMR ($CD_3CN$): $\delta$ = 174.3 ($Me_2C$=N), 152.8 (Ar), 143.0 ($C_3$pz), 133.3 ($C_5$pz), 131.6 (Ar), 128.5 (Ar), 121.2 (Ar), 107.4 ($C_4$pz), 76.4 ($C_{meth}$), 29.6 ($CH_3$), 21.1 ($CH_3$) ppm.

**[Ag(L1)](OTf) (4):** A solution of **L1** (0.201 g, 0.840 mmol) in THF (10 mL) was added to a solution of Ag(OTf) (0.216 g, 0.840 mmol) in THF (10 mL). The flask that had originally contained **L1** was washed with additional THF (5 mL), which was transferred into the reaction mixture. A colorless precipitate formed immediately. After the resulting solution had been stirred at room temperature for 2 h, solvent was removed by cannula filtration. The residue was washed with $Et_2O$ (two 5 mL portions) and dried under vacuum to leave **2** (0.376 g, 90 %) as a colorless solid, m.p. 161–162 °C (decomposed). $^1$H NMR ($CD_3CN$): $\delta$ = 7.94 (d, *J* = 2.4 Hz, 2 H, pz), 7.74 (s, 1 H, CH), 7.58 (d, *J* = 1.8 Hz, 2 H, pz), 6.61 (dt, *J* = 8.7, 2.1 Hz, 2 H, Ar), 6.45 (d, *J* = 8.7 Hz, 2 H, Ar), 6.43 (dd, *J* = 2.5, 1.9 Hz, 2 H, pz), 4.40 (s, 2 H, $NH_2$) ppm. $^{13}$C NMR ($CD_3CN$): $\delta$ = 150.0 ($C_{1or4}$Ar), 142.9 ($C_3$pz), 133.4 ($C_5$pz), 128.9 ($C_{3,5}$Ar), 124.1 ($C_{4or1}$Ar), 115.1 ($C_{2,6}$Ar), 107.2 ($C_4$pz), 76.9 ($C_{meth}$) ppm. $^{19}$F NMR ($CD_3CN$): $\delta$ = –79.34 ppm. IR (KBr): $\tilde{\nu}_{NH}$ = 3274, 3167 cm$^{-1}$. $C_{14}H_{13}N_5O_3SF_3Ag$: calcd. (found) C 33.89 (34.14), H 2.64 (2.56), N 14.11 (14.16). Crystals suitable for X-ray diffraction can be grown by vapor diffusion of $Et_2O$ into a $CH_3CN$ solution of **4** (30 mg in 1 mL) or by mixing acetone solutions of **L** and AgOTf and letting the solution sit undisturbed overnight.

**[Ag(L1)]($NO_3$) (5):** A solution of **L$_2$** (0.212 g, 0.885 mmol) in THF (10 mL) was added to a solution of Ag($NO_3$) (0.150 g, 0.885 mmol) in THF (10 mL). After the resulting solution had been stirred at room temperature for 12 h, solvent was removed by cannula filtration. The residue was washed with $Et_2O$ (two 5 mL portions) and dried under vacuum to leave **4** (0.313 g, 86 %) as a colorless solid, m.p. 158–159 °C (decomposed). $^1$H NMR ($CD_3CN$): $\delta$ = 7.98 (dd, *J* = 2.5, 0.5 Hz, 2 H, pz), 7.82 (s, 1 H, CH), 7.60 (d, *J* = 1.9 Hz, 2 H, pz), 6.61 (d, *J* = 8.6 Hz, 2 H, Ar), 6.45 (d, *J* = 8.6 Hz, 2 H, Ar), 6.43 (t, *J* = 2.2 Hz, 2 H, pz), 4.43 (s, 2 H, $NH_2$) ppm. $^{13}$C NMR ($CD_3CN$): $\delta$ = 150.0 ($C_{1\ or\ 4}$Ar), 142.9 ($C_3$pz), 133.4 ($C_5$pz), 128.9 ($C_{3,5}$Ar), 124.2 ($C_{4\ or\ 1}$Ar), 115.1 ($C_{2,6}$Ar), 107.2 ($C_4$pz), 76.9 ($C_{meth}$) ppm. IR (KBr): $\tilde{\nu}_{NH}$ = 3263, 3131 cm$^{-1}$. $C_{13}H_{13}N_6AgO_3$: calcd. (found) C 38.16 (38.17), H 3.20 (3.27), N 20.54 (20.47). Crystals of **5**·0.25 $H_2O$·*x* ($Et_2O$/$CH_3CN$) (here referred to simply as **5**·0.25 $H_2O$; see crystallographic section for

further details) were grown by vapor diffusion of $Et_2O$ into a solution of **5** in $CH_3CN$. The hydrate water presumably originated from atmospheric moisture.

## Crystallography

X-ray intensity data from a colorless plate of **L1**, a colorless needle of **[Ag(L1)](BF$_4$)** (**1**), a light yellow prism of **[Ag(L1)(CH$_3$CN)$_{0.25}$](BF$_4$)** (**1**·0.25 $CH_3CN$), a colorless prism of **[Ag(L1)(CH$_3$CN)$_{0.125}$](PF$_6$)** (**2**·0.125 $CH_3CN$), a colorless plate of **[Ag(L1)(CH$_3$CN)](PF$_6$)** (**2**·$CH_3CN$), a colorless plate of **[Ag(L2)](PF$_6$)** (**3**), a colorless block of **[Ag(L1)](OTf)** (**4**), and a colorless needle of **[Ag(L1)](NO$_3$)**·0.25 $H_2O$·*x* ($Et_2O$/$CH_3CN$) [**5**·0.25 $H_2O$·*x* ($Et_2O$/$CH_3CN$), again, henceforth referred to as **5**·0.25 $H_2O$] were collected at 100.0(1) K with an Oxford Diffraction Ltd. Supernova diffractometer equipped with a 135 mm Atlas CCD detector and use of Cu-$K_\alpha$ for **1** and **5**·0.25 $H_2O$ and Mo-$K_\alpha$ radiation for the other experiments. Raw data frame integration and Lp corrections were performed with either CrysAlis Pro (Oxford Diffraction, Ltd.)**33** or SAINT+ (Bruker).**34** Final unit cell parameters were determined by least-squares refinement of 3095, 6061, 16641, 10576, 22553, 9664, 7558, and 9167 reflections for **L1**, **1**, **1**·0.25 $CH_3CN$, **2**·0.125 $CH_3CN$, **2**·$CH_3CN$, **3**, **4**, and **5**·0.25 $H_2O$, respectively, with $I > 2\sigma(I)$ in each case. Analysis of the data showed negligible crystal decay during collection in each case. Direct methods, structure solutions, difference Fourier calculations, and full-matrix, least-squares refinements against $F^2$ were performed with SHELXTL.**35** An empirical absorption correction using spherical harmonics, implemented in the SCALE3 ABSPACK**36** scaling algorithm, was applied to the data for **L1**, **2**·0.12 $CH_3CN$, and **5**·0.25 $H_2O$ whereas numerical absorption corrections based on Gaussian integration over a multifaceted crystal model were applied to the data for the other crystals. With the exception of the isotropic refinement for atoms of the disordered acetonitrile, $PF_6$, and phenyl ring atoms in **2**·0.125 $CH_3CN$, all non-hydrogen atoms were refined with anisotropic displacement parameters. Hydrogen atoms were placed in geometrically idealized positions and included as riding atoms. The crystal of **2**·0.125 $CH_3CN$ was a regular twin with 180° rotation around [110]. The crystal of **5**·0.25 $H_2O$ was of low quality and was a regular 1:1 twin in which the components were related by a 180° rotation about the *x** axis. One of the components was also cracked unevenly (in a 2:3 ratio) with an angle $\alpha \approx 5°$ separating these parts. Because of partial occupancy (desolvation), disorder, and twinning, a solvent mask (SQUEEZE)**37** that generated 156.9 Å$^3$ voids corresponding to 5.1 % of the unit cell volume (3102.2 Å$^3$) was applied. Unfortunately the exact composition of solvent in the voids could not be identified because the solvent mask procedure is incompatible with the twin refinement by HKLF5. The X-ray crystallographic parameters and further details of data collection and structure refinements are given in Tables S1 and S2 in the Supporting Information.

CCDC-1419374 (for **L1**), -1419375 (for **1**), -1419376 (for **1**·0.25 $CH_3CN$), -1419377(for **2**·0.125 $CH_3CN$), -1419378 (for **2**·$CH_3CN$), -1419379 (for **3**), -1419380 (for **4**), and -1419381 (for **5**·0.25 $H_2O$) contain the supplementary crystallographic data for this paper. These data can be obtained free of charge from The Cambridge Crystallographic Data Centre via **www.ccdc.cam.ac.uk/data_request/cif**.

# Acknowledgements

J. R. G. thanks Marquette University and the US National Science Foundation (NSF) (CHE-0848515) for support. N. B. S. acknowledges support by Advanced Support for Innovative Research Excellence (ASPIRE-I and -III grants). D. E. W. was partially supported by Support to Promote Advancement of Research and Creativity (SPARC).

## References


1 P. Thanasekaran, T.-T. Luo, C.-H. Lee and K.-L. Lu, *J. Mater. Chem.*, 2011, **21**, 13140– 13149.

2 X. Wu, N. Ding, W. Zhang, F. Xue, T. S. A. Hor Inorg. Chem. 2015, ASAP; N. Lopez, H. Zhao, D. Zhao, H.-C. Zhou and J. P. Riebenspies, *Dalton Trans.*, 2013, **42**, 54– 57.

3 M.-J. Dong, M. Zhao, S. Ou, C. Zou and C.-D. Wu, *Angew. Chem. Int. Ed.*, 2014, **53**, 1575– 1579; *Angew. Chem.*, 2014, **126**, 1601.

4 G.-Q. Kong, S. Ou, C. Zou and C.-D. Wu, *J. Am. Chem. Soc.*, 2012, **134**, 19851– 19857.

5 N. N. Adarsh, M. M. Dîrtu, A. D. Naik, A. F. Léonard, N. Campagnol, K. Robeyns, J. Snauwaert, J. Fransaer, B. L. Su and Y. Garcia, *Chem. Eur. J.*, 2015, **21**, 4300– 4307.

6 M. Yoon, K. Suh, S. Natarajan and K. Kim, *Angew. Chem. Int. Ed.*, 2013, **52**, 2688– 2700; *Angew. Chem.*, 2013, **125**, 2752; T. Panda, T. Kundu and R. Banerjee, *Chem. Commun.*, 2012, **48**, 5464– 5466.

7 A. Ienco, M. Caporali, F. Costantino, A. Guerri, G. Manca, S. Moneti and M. Peruzzini, *J. Coord. Chem.*, 2014, **67**, 3863– 3872.

8 C. R. Murdock and D. M. Jenkins, *J. Am. Chem. Soc.*, 2014, **136**, 10983– 10988; C. R. Murdock, N. W. McNutt, D. J. Keffer and D. M. Jenkins, *J. Am. Chem. Soc.*, 2014, **136**, 671– 678; G. Wu, J. Bai, Y. Jiang, G. Li, J. Huang, Y. Li, C. E. Anson, A. K. Powell and S. Qiu, *J. Am. Chem. Soc.*, 2013, **135**, 18276– 18279.

9 J. de Groot, K. Gojdas, D. K. Unruh and T. Z. Forbes, *Cryst. Growth Des.*, 2014, **14**, 1357– 1365; J.-Y. Wu, Y.-C. Liu and T.-C. Chao, *Inorg. Chem.*, 2014, **53**, 5581– 5588.

10 T. Bataille, S. Bracco, A. Comotti, F. Costantino, A. Guerri, A. Ienco and F. Marmottini, *CrystEngComm*, 2012, **14**, 7170– 7173; T. Bataille, F. Costantino, P. Lorenzo-Luis, S. Midollini and A. Orlandini, *Inorg. Chim. Acta*, 2008, **361**, 327– 334.

11 L. S. Shimizu, S. R. Salpage and A. A. Korous, *Acc. Chem. Res.*, 2014, **47**, 2116– 2127; Z. Liu, G. Liu, Y. Wu, D. Cao, J. Sun, S. T. Schneebeli, M. S. Nassar, C. A. Mirkin and J. F. Stoddart, *J. Am. Chem. Soc.*, 2014, **136**, 16651– 16660; B. Gong and Z. Shao, *Acc. Chem. Res.*, 2013, **46**, 2856– 2866.

12 G. Durá, M. C. Carrión, F. A. Jalón, A. M. Rodríguez and B. R. Manzano, *Cryst. Growth Des.*, 2014, **14**, 3510– 3529; G. Durá, M. C. Carrión, F. A. Jalón, A. M. Rodríguez and B. R. Manzano, *Cryst. Growth Des.*, 2013, **13**, 3275– 3282; M. C. Carrión, G. Durá, F. A. Jalón, B. R. Manzano and A. M. Rodríguez, *Cryst. Growth Des.*, 2012, **12**, 1952– 1969.

13 I. Bassanetti, A. Comotti, P. Sozzani, S. Bracco, G. Calestani, F. Mezzadri and L. Marchiò, *J. Am. Chem. Soc.*, 2014, **136**, 14883– 14895; I. Bassanetti, F. Mezzadri, A. Comotti, P. Sozzani, M. Gennari, G. Calestani and L. Marchiò, *J. Am. Chem. Soc.*, 2012, **134**, 9142– 9145; I. Bassanetti and L. Marchiò, *Inorg. Chem.*, 2011, **50**, 10786– 10797.

14 G. A. Santillan and C. J. Carrano, *Dalton Trans.*, 2009, 6599– 6605; G. A. Santillan and C. J. Carrano, *Cryst. Growth Des.*, 2009, **9**, 1590– 1598; G. A. Santillan and C. J. Carrano, *Inorg. Chem.*, 2008, **47**, 930– 939; G. A. Santillan and C. J. Carrano, *Dalton Trans.*, 2008, 3995– 4005.

15 J. R. Gardinier, J. S. Hewage and S. V. Lindeman, *Inorg. Chem.*, 2014, **53**, 12108– 12121.

16 a) K. I. Thé and L. K. Peterson, *Can. J. Chem.*, 1973, **51**, 422– 426; b) K. I. Thé, L. K. Peterson and E. Kiehlmann, *Can. J. Chem.*, 1973, **51**, 2448– 2451; c) L. K. Peterson, E. Kiehlmann, A. R. Sanger and K. I. Thé, *Can. J. Chem.*, 1974, **52**, 2367– 2374.

17 K. Kimura, J.-H. Zhuang, M. Kida, Y. Yamashita and Y. Sakaguchi, *Polym. J. (Tokyo)*, 2003, **35**, 455– 459; M. Jeffries-El, B. D. Benneyworth and R. M. Tarkka, *Polym. Prepr. Am. Chem. Soc. Div. Polym. Chem.*, 2000, **41**, 174– 175; R. S. Tsekhanskii and V. F. Ushenina, *Izv. Vyssh. Uchebn. Zaved. Khim. Khim. Tekhnol.*, 1975, **18**, 1830; G. F. D'Alelio, W. F. Strazik and T. F. Huemmer, *J. Macromol. Sci. Chem.*, 1968, **2**, 335– 365; H. A. Smith, W. K. Carrington, US

patent, 3418281A, 19681224; J. J. Blanksma, *Chemisch Weekblad*, 1913, **9**, 862– 870; P. Cohn and L. Springer, *Monatsh. Chem.*, 1903, **24**, 87– 100.
18 M. C. Carrión, F. A. Jalón, B. R. Manzano, A. M. Rodríguez, F. Sepúlveda and M. Maestro, *Eur. J. Inorg. Chem.*., 2007, 3961– 3973.
19 B. Y.-W. Man, M. Bhadbhade and B. A. Messerle, *New J. Chem.*, 2011, **35**, 1730– 1739; B. J. Liddle and J. R. Gardinier, *J. Org. Chem.*, 2007, **72**, 9794– 9797.
20 L. Hu, S. Yan, Z. Luo, X. Han, Y. Wang, Z. Wang and C. Zeng, *Molecules*, 2012, **17**, 10652– 10666; G. Biagi, G. Dell'omodarme, M. Ferretti, I. Giorgi, O. Livi and V. Scartoni, *Farmaco*, 1992, **47**, 335– 344.
21 B. J. Liddle, D. Hall, S. V. Lindeman, M. D. Smith and J. R. Gardinier, *Inorg. Chem.*, 2009, **48**, 8404– 8414.
22 T. L. Davis, J. L. Watts, K. J. Brown, J. S. Hewage, A. R. Treleven, S. V. Lindeman, J. R. Gardinier *Dalton Trans*, **2015**, Advance Article, DOI: 10.1039/C5DT02773J.
23 M. H. Reineke, M. D. Sampson, A. L. Rheingold and C. P. Kubiak, *Inorg. Chem.*, 2015, **54**, 3211– 3217.
24 L. Yang, D. R. Powell and R. P. Houser, *Dalton Trans.*, 2007, 955– 964.
25 F. Grepioni, G. Cojazzi, S. M. Draper, N. Scully and D. Braga, *Organometallics*, 1998, **17**, 296– 307.
26 A. R. Choudhury and T. N. G. Row, *Cryst. Growth Des.*, 2004, **4**, 47– 52; J. A. van den Berg and K. R. Seddon, *Cryst. Growth Des.*, 2003, **3**, 643; L. Brammer, E. A. Bruton and P. Sherwood, *New J. Chem.*, 1999, **23**, 965– 968; V. R. Thalladi, H.-C. Weiss, D. Bläser, R. Boese, A. Nangia and G. R. Desiraju, *J. Am. Chem. Soc.*, 1998, **120**, 8702– 8710.
27 R. K. Castellano, F. Diederich and E. A. Meyer, *Angew. Chem. Int. Ed.*, 2003, **42**, 1210– 1250; *Angew. Chem.*, 2003, **115**, 1244; C. J. Janiak, *J. Chem. Soc., Dalton Trans.*, 2000, 3885– 3896.
28 M. Kaźmierczak and A. Katrusiak, *Cryst. Growth Des.*, 2014, **14**, 2223– 2229.
29 J. Bernstein, *Cryst. Growth Des.*, 2013, **13**, 961– 964; C. R. Jones, P. K. Baruah, A. L. Thompson, S. Scheiner and M. D. Smith, *J. Am. Chem. Soc.*, 2012, **134**, 12064– 12071; Y. Gu, T. Kar and S. Scheiner, *J. Am. Chem. Soc.*, 1999, **121**, 9411– 9422; G. J. Desiraju, *Acc. Chem. Res.*, 1996, **29**, 441– 449; T. Steiner and F. Saenger, *J. Am. Chem. Soc.*, 1992, **114**, 10146– 10154; G. J. Desiraju, *Acc. Chem. Res.*, 1991, **24**, 290– 296; R. Taylor and O. Kennard, *J. Am. Chem. Soc.*, 1982, **104**, 5063– 5070.
30 H. Takahashi, S. Tsuboyama, Y. Umezawa, K. Honda and M. Nishio, *Tetrahedron*, 2000, **56**, 6185– 6191; S. Tsuzuki, K. Honda, T. Uchimaru, M. Mikami and K. Tanabe, *J. Am. Chem. Soc.*, 2000, **122**, 11450– 11458; M. Nishio, M. Hirota and Y. Umezawa, in: *The CH-π interaction: evidence, nature, and consequences*, Wiley-VCH, New York, 1998; Y. Umezawa, S. Tsuboyama, K. Honda, J. Uzawa and M. Nishio, *Bull. Chem. Soc. Jpn.*, 1998, **71**, 1207– 1213; D. Braga, F. Grepioni and E. Tedesco, *Organometallics*, 1998, **17**, 2669– 2672.
31 D. L. Reger, R. F. Semeniuc and M. D. Smith, *Cryst. Growth Des.*, 2005, **5**, 1181– 1190.
32 A. Salis and B. W. Ninham, *Chem. Soc. Rev.*, 2014, **43**, 7358– 7377; R. Díaz-Torres and S. Alvarez, *Dalton Trans.*, 2011, **40**, 10742– 10750.
33 *CrysAlisPro*, Agilent Technologies, version 1.171.34.46 (release 25–11–2010, CrysAlis171.NET, compiled Nov. 25 2010, 17:55:46).
34 SAINT+, version 7.23a and SADABS, version 2004/1, Bruker Analytical X-ray Systems, Inc., Madison, Wisconsin, USA, **2005**.
35 G. M. Sheldrick, SHELXTL, version 6.12, Bruker Analytical X-ray Systems, Inc., Madison, Wisconsin, USA, 2001.

36 *SCALE3 ABSPACK – An Oxford Diffraction program* (1.0.4, gui: 1.0.3) (C), Oxford Diffraction Ltd., **2005**.
37 A. L. Spek, *Acta Crystallogr., Sect. C*, 2015, **71**, 9– 18.